Fusion Engineering and Design 88 (2013) 413–420

Contents lists available at SciVerse ScienceDirect

Fusion Engineering and Design

journal homepage: www.elsevier.com/locate/fusengdes

Study on three-dimensional heterogeneous calculation of ITER test blanket module with deterministic method

Guangchun Zhang, Hongchun Wu, Liangzhi Cao*, Youqi Zheng, Yunzhao Li, Zhouyu Liu

School of Nuclear Science and Technology, Xi'an Jiaotong University, Xi'an, Shaanxi 710049, China

HIGHLIGHTS

- A new code system based on the two-step approach for the neutronics analysis of the test blanket module (TBM) for ITER is developed.
- The code system can perform the neutronics analysis based on precise geometry.
- A new developed 3D modular ray tracing technique is adopted.
- The numerical results indicate that the code system is reliable and efficient for the conceptual design of TBM.

ARTICLE INFO

Article history:
Received 17 June 2012
Received in revised form 27 February 2013
Accepted 8 April 2013
Available online 4 May 2013

Keywords:
Deterministic method
Methods of characteristics
Simplified spherical harmonics
Neutronics
ITER
Test blanket module

ABSTRACT

The neutronics analysis on the test blanket module (TBM) has important significance for the ITER device and its related experiment design. Quantities of scoping-type studies and conceptual designs were published by using the Monte Carlo method. However, disadvantages like time consuming make it necessary to develop a new highly efficient method. Hence, a new two-step approach method based on the 3D deterministic method for analyzing the TBM is proposed in this paper. A code package 3DMOC-NSPn was developed. It is mainly composed of three modules, the 3DMOC for generating the homogenization cross section; the LINK code for cross section condensation and the NSPn code for blanket calculation. The detailed flux distribution throughout the whole TBM and the mainly neutronics features, such as TBR, displacement per atom (DPA), helium and hydrogen production rate can be obtained. To validate the numerical approach and the code package, the calculations on China dual functional lithium lead-test blanket module (DFLL-TBM) was performed. The reference results were obtained by using the MCNP code. The numerical results from 3DMOC-NSPn are in good agreement with the references. It indicates that the whole code package is a reliable neutronics analysis tool for the TBM design and evaluation.

1. Introduction

Neutronics analyses of the ITER test blanket module (TBM) are very important for the design, construction and experiment of ITER. Quantities of scoping-type studies and conceptual blanket designs were mainly based on the Monte Carlo codes, adopting point wise cross-section data library [1]. The MCNP code is the most widely used calculation tool in the neutronics analysis [2–4] while the MCNPX code has also been used [5]. Some CAD Interface codes and conversion codes that are used to convert the CAD data into the semi-algebraic representation used by MCNP were developed [6–8].

Although the MCNP code has given the satisfying results, there are still some disadvantages. In the MCNP calculation, several runs are needed to get the ultimate results, which require different variance reduction techniques for each response under consideration. But variance reduction techniques usually cause increased computer time [9]. Moreover the application of variance reduction techniques is usually difficult especially in some deep penetration problems that require the effective use of variance reduction techniques in order to achieve reliable results. In addition, a huge number of histories are needed in the MCNP calculations for the large size problems and it will increase the computer time significantly. Meanwhile the large size model brings the deep penetration problem in which the MCNP calculation is usually not so satisfying [10].

Deterministic methods are always more efficient than Monte Carlo methods, and thus are widely used and well developed in neutronics analyses of traditional fission reactors. However, most deterministic methods are limited by their geometry adaptabilities, especially for those complex systems like ITER TBM. Recently, an advanced deterministic methods called method of characteristic (MOC) is widely studied because of its high geometry adaptability. But most of those studies are based on 2D model. Direct MOC calculations for 3D problems require a tremendous amount of memory

* Corresponding author. Tel.: +86 29 8266 3285; fax: +86 29 8266 8916.
E-mail addresses: caolz@mail.xjtu.edu.cn, caoliangzhi@gmail.com (L. Cao).

0920-3796/$ – see front matter © 2013 Elsevier B.V. All rights reserved.
http://dx.doi.org/10.1016/j.fusengdes.2013.04.019

[11] and very long computing time. As one solution, a 2D + 1D strategy is proposed, which combines 2D MOC for the radial calculation and 1D calculation in the axial direction. This method performs well when the geometry keeps the same in the axial direction [12]. But it is not easy to apply it to the problems with unstructured axial geometry, such as the TBM of ITER. Hence the 2D + 1D method is not adopted in this paper.

To overcome above difficulties, this paper proposes a two-step approach which is widely used and proven to be very efficient for light water reactors. For the first step, the TBM is dissected to several different typical units, "lattice calculations" are performed on these units to get the homogenous cross sections; For the second step, transport calculations are performed on the whole TBM to get the full flux mapping everywhere. Based on this approach, a code package 3DMOC-NSPn was developed. It is mainly composed of three modules, the 3DMOC for generating the homogenization cross section; the LINK code for homogenized cross section condensation, and the NSPn code for blanket module calculation. Different from MCNP code, this new developed code package has the advantage of providing a full flux mapping everywhere in one run.

To validate the numerical approach and the code package, calculations on DFLL-TBM were performed. The reference results were obtained by using the MCNP code. The nuclear databases, which are basically constructed from the Fusion Evaluated Data Library FENDL-2.1, either in multi-group (MG/GENDF, MG/MATXS) or Monte Carlo point wise data (MC/FEDNL2.1) are the reference databases. The overview of the DFLL-TBM program can be found in Ref. [13].

The remainder of this paper is organized as follows. Section 2 presents the methodology of this work, including the model, the mathematical derivation and the details in calculation codes. Section 3 is dedicated to some numerical results with comparison to Monte Carlo code. Finally, the results are summarized and discussed in Section 4.

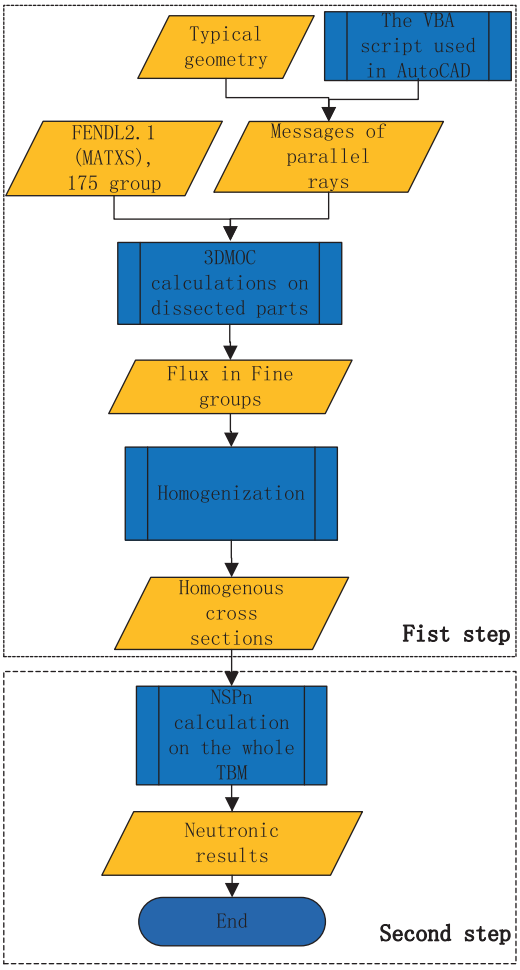

Fig. 1. Flow chart of the whole calculation scheme.

2. Computational scheme and codes

The main difficulties faced by 3D deterministic calculations for ITER TBM are the large scale of TBM and the large number of the energy group in FENDL library. It is too time consuming if the 175-group structure is applied directly to the whole TBM calculation. Considering this, the homogenization technique is adopted to get the final flux distribution throughout the TBM and it proceeds in two steps. As shown in Fig. 1, the first step is to dissect the realistic 3D heterogeneous model into several typical independent parts. Transport calculations are performed on these typical parts respectively with 3DMOC code adopting FENDL/MG-2.1 library to get detailed heterogeneous spatial flux distribution, followed by the use of the flux distribution to condense the 175 energy group structure to a smaller, more manageable energy group structure. Then in the second step, the NSPn code is used to calculate the flux distribution and some other neutronic results throughout the whole TBM. During the computation process, the calculation model is also realistic 3D heterogeneous and all cross section messages are from the data library generated in the first step.

2.1. The FENDL2.1 cross-section library

The data libraries FENDL/MG-2.1 and FENDL/MC-2.1 contain cross section data in multigroup and continuous-energy ACE format respectively, derived from FENDL/E-2.1, a library of selected evaluated neutron–nucleus and photon–atom interaction cross-sections for nuclides of importance for neutron–photon transport calculations for fusion reactor design, in the energy range from 10^{-5} eV up to 20 MeV [14]. The FENDL/MC-2.1 library which contains neutron pointwise cross section data files is used in the MCNP run in this present paper. The BBC and TRANSX processing codes are used to generate 175 group cross sections which are used in the 3DMOC calculation from the multigroup library FENDL/MG-2.1 [15].

2.2. The 3DMOC code

Due to the complicated and unstructured geometry of TBM, the calculation code should have the advantage of geometry flexibility. The MOC is an effective tool for neutron transport calculations. It considers only a finite number of discrete directions (with quadrature sets) and calculates mesh average angular flux by sweeping. For a given direction, each of several parallel rays is traced to provide mesh-average ray angular flux and outgoing ray angular flux by analytic integration along the tracing ray. The ray-wise integration allows flexibility of the mesh shapes. It can take any shape and mixture of shapes as in Monte Carlo methods. Hence, the MOC method is extremely suitable for analyzing the TBM due to its geometry flexibility.

The basic idea of MOC is described as follows: the Boltzmann transport equation describing the neutron transport behavior can be written in the following form along the path, namely the characteristics.

$$\frac{d\phi_g(s,\vec{\Omega}_m)}{ds} + \Sigma_{t,g}(s)\phi_g(s,\vec{\Omega}_m) = Q_g(s,\vec{\Omega}_m) \quad (1)$$

The source consists of the scattering and fission parts:

$$Q_g(s,\vec{\Omega}) = \frac{1}{4\pi}\sum_{g'}\Sigma_{s,g'\to g}(s)\bar{\phi}_{g'}(s) + \frac{\chi_g}{4\pi k_{eff}}\sum_{g'}\nu\Sigma_{f,g'}(s)\bar{\phi}_{g'}(s) \quad (2)$$

After the domain is divided into some sub-domains and both the material and the neutron source are assumed to be flat, the outgoing angular flux from sub-domain i along the path k and be given by

$$\phi^{out}_{g,i,k}(\vec{\Omega}_m) = \phi^{in}_{g,i,k}(\vec{\Omega}_m)\exp(-\Sigma_{t,g,i}s_{i,k}) + \frac{Q_{g,i}(\vec{\Omega}_m)}{\Sigma_{t,g,i}}[1-\exp(-\Sigma_{t,g,i}s_{i,k})] \quad (3)$$

where $s_{i,k}$ is the traveling distance in the sub-domain i of the path k; and $\phi^{in}_{g,i,k}(\vec{\Omega}_m)$ is the incoming angular flux.

The average angular flux of the segment i, k $\bar{\phi}_{g,i,k}(\vec{\Omega}_m)$ can be obtained by integrating Eq. (3) along the path k:

$$\bar{\phi}_{g,i,k}(\vec{\Omega}_m) = \frac{Q_{g,i}(\vec{\Omega}_m)}{\Sigma_{t,g,i}} + \frac{\phi^{in}_{g,i,k}(\vec{\Omega}_m) - \phi^{out}_{g,i,k}(\vec{\Omega}_m)}{\Sigma_{t,g,i}s_{i,k}} \quad (4)$$

The sub-domain average angular flux $\bar{\phi}_{g,i}(\vec{\Omega}_m)$ is given by:

$$\bar{\phi}_{g,i}(\vec{\Omega}_m) = \frac{\Sigma_k\bar{\phi}_{g,i,k}(\vec{\Omega}_m)s_{i,k}\delta A_k}{\Sigma_k s_{i,k}\delta A_k} \quad (5)$$

In addition, the traveling distance should be corrected since the numerical calculated volume $\Sigma_k s_{i,k}\delta A_k$ is not equal to the true volume V_i:

$$s'_{i,k} = s_{i,k}\frac{V_i}{\Sigma_k s_{i,k}\delta A_k} \quad (6)$$

The 3DMOC code is a coupling of 3D method of characteristics and the common geometry module [16]. This arrangement allows CAD models to be analyzed without using the common approach of surface equations or Boolean operations in the input card. The information of characteristic rays can be generated in AutoCAD code automatically by a VBA script. It will significantly eliminate human errors in preparing geometry input and preserve the exact geometry details.

Because of the heterogeneity of the TBM in the axial direction, a realistic 3D code is needed. However, direct MOC calculations for 3D problems require a tremendous amount of memory and very long computing time. Therefore, a 3D modular ray tracing technique [16] is adopted in the 3DMOC code, which can not only hold the geometry flexibility of the MOC but also reduce the tremendous memory requirement. For the modular ray tracing technique, the object geometry is dissected into many cuboid cells by a background mesh. Typical geometric cells are picked out and ray traced. Only in these typical cells, the ray tracing data is stored.

The scheme of the 3D modular ray tracing technique for the MOC is shown in Fig. 2 [16].

2.3. The homogenization technique

The traditional homogenization technique usually proceeds in two steps: a lattice transport calculation to obtain the detailed heterogeneous flux distribution, flowed by the use of this detailed flux distribution to calculate average homogeneous cross sections.

The homogenized cross sections are defined as follow:

$$\Sigma_{t,G,I} = \frac{\sum_{i\in I}\sum_{g\in G}\Sigma_{t,g,i}\varphi_{g,i}V_i}{\sum_{i\in I}\sum_{g\in G}\varphi_{g,i}V_i} \quad (7a)$$

$$\Sigma_{a,G,I} = \frac{\sum_{i\in I}\sum_{g\in G}\Sigma_{a,g,i}\varphi_{g,i}V_i}{\sum_{i\in I}\sum_{g\in G}\varphi_{g,i}V_i} \quad (7b)$$

$$\Sigma_{s,G'\to G,I} = \frac{\sum_{i\in I}\sum_{g\in G}\sum_{g\in G'}\Sigma_{s,g'\to g,i}\varphi_{g',i}V_i}{\sum_{i\in I}\sum_{g'\in G}\varphi_{g',i}V_i} \quad (7c)$$

where $\varphi_{g,i}$ is the scalar flux of region i and fine group g; V_i is the volume of region i; $\Sigma_{a,g,i}$, $\Sigma_{t,g,i}$ and $\Sigma_{s,g'\to g,i}$ are the absorption cross section, total cross section and scattering cross section of fine group g, respectively. $\Sigma_{a,G,i}$, $\Sigma_{t,G,i}$ and $\Sigma_{s,G'\to G,i}$ are the absorption cross section, total cross section and scattering cross section of coarse group G and coarse region I, respectively.

2.4. The NSPn code

Due to the time-consuming problem faced by the 3D deterministic calculation performed on large scale problems, a smart method is needed to give good accuracy within a realistic computing cost. The simplified P_N equations were originally proposed by Gelbard [17]. Through the years many researchers have investigated the accuracy of these equations and found them to render approximate transport solutions which are more accurate than diffusion theory, but significantly less expensive than discrete-ordinates (S_N) or full P_N solutions. Nonetheless, a lack of mathematical rigor in the original derivation of the SP_N equations had hindered the widespread use of these equations for a long period until Larsen and colleagues showed that the SP_N equations represent a rigorous asymptotic approximation to the transport equation in the classical diffusion limit [18].

In the NSPn code used in this paper, the SP_3 method is adopted to treat the angular variable and the Nodal method is adopted to treat the spatial variables. This arrangement could reduce computer run time significantly.

The multigroup SP_3 equations solved in NSPn code are derived from the monodimensional multigroup P_3 equations (Eq. (8)), assuming isotropic source and isotropic scattering:

$$-\frac{d\psi^1_g}{dx} + \Sigma_{t,g}\psi^0_g = \sum_{g'}\Sigma_{s,g'\to g}\psi^0_{g'} + \frac{\chi_g}{k_{eff}}\sum_{g'}\nu\Sigma_{f,g'}\psi^0_{g'} \quad (8a)$$

$$-\frac{d\psi^0_g}{dx} - 2\frac{d\psi^2_g}{dx} + 3\Sigma_{t,g}\psi^1_g = 0 \quad (8b)$$

$$-2\frac{d\psi^1_g}{dx} - 3\frac{d\psi^3_g}{dx} + 5\Sigma_{t,g}\psi^2_g = 0 \quad (8c)$$

$$-3\frac{d\psi^2_g}{dx} + 7\Sigma_{t,g}\psi^3_g = 0 \quad (8d)$$

The notation in Eq. (8) is standard: x is the spatial variable; ψ^0_g, ψ^1_g, ψ^2_g and ψ^3_g are the flux moments; $\Sigma_{t,g}$ is the total cross section of group g, $\Sigma_{s,g'\to g}$ is the scattering cross section from group g to group g', $\Sigma_{f,g'}$ is the fission cross section of g'.

Eliminate all odd-order moments from Eq. (8), one obtains:

$$\begin{cases} -\left(\frac{1}{3\Sigma_{t,g}}\cdot\frac{d^2\psi^0_g}{dx^2} + \frac{2}{3\Sigma_{t,g}}\cdot\frac{d^2\psi^2_g}{dx^2}\right) + \Sigma_{t,g}\psi^0_g = \sum_{g'}\Sigma_{s,g'\to g}\psi^0_{g'} + \frac{\chi_g}{k_{eff}}\sum_{g'}\nu\Sigma_{f,g'}\psi^0_{g'} \\ -2\left(\frac{1}{3\Sigma_{t,g}}\cdot\frac{d^2\psi^0_g}{dx^2} + \frac{2}{3\Sigma_{t,g}}\cdot\frac{d^2\psi^2_g}{dx^2}\right) - 3\cdot\frac{3}{7\Sigma_{t,g}}\cdot\frac{d^2\psi^2_g}{dx^2} + 5\Sigma_{t,g}\psi^2_g = 0 \end{cases} \quad (9)$$

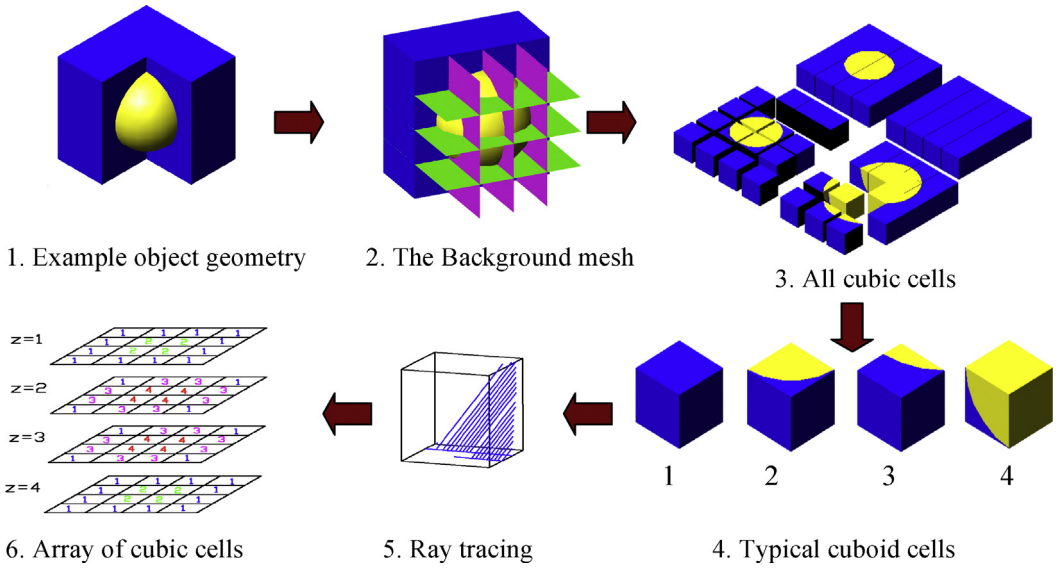

Fig. 2. Modular ray tracing process.

Substitute the d^2/dx^2 with ∇^2, one obtains the following SP_3 equations:

$$\begin{cases} -D_g \cdot \nabla^2(\psi_g^0 + 2\psi_g^2) + \Sigma_{r,g}(\psi_g^0 + 2\psi_g^2) = S_g + 2\Sigma_{r,g}\psi_g^2 \\ -\frac{27}{35}D_g \cdot \nabla^2\psi_g^2 + \Sigma_{t,g}\psi_g^2 = \frac{2}{5}(\Sigma_{r,g}\psi_g^0 - S_g) \end{cases} \quad (10)$$

where

$$D_g = \frac{1}{3\Sigma_{t,g}}, \quad \Sigma_{r,g} = \Sigma_{t,g} - \Sigma_{s,g\to g} \quad (11a)$$

$$S_g = \sum_{g' \neq g} \Sigma_{s,g'\to g}\psi_{g'}^0 + \frac{\chi_g}{k_{eff}}\sum_{g'} \nu\Sigma_{f,g'}\psi_{g'}^0 \quad (11b)$$

Some manipulations give

$$\begin{cases} \nabla^2\Phi_g - (\kappa_g^0)^2\Phi_g = -\frac{1}{D_g^0}S_g^0 \\ \nabla^2\psi_g^2 - (\kappa_g^2)^2\psi_g^2 = -\frac{1}{D_g^2}S_g^2 \end{cases} \quad (12)$$

where

$$\Phi_g = \psi_g^0 + 2\psi_g^2 \quad (13a)$$

$$D_g^0 = D_g, \quad D_g^2 = \frac{27}{35}D_g \quad (13b)$$

$$\kappa_g^0 = \sqrt{\frac{\Sigma_{r,g}}{D_g^0}}, \quad \kappa_g^2 = \sqrt{\frac{\Sigma_{t,g}}{D_g^2}} \quad (13c)$$

$$S_g^0 = S + 2\Sigma_{r,g}\psi_g^2, \quad S_g^2 = \frac{2}{5}(\Sigma_{r,g}\psi_g^0 - S) \quad (13d)$$

Then the Nodal method which is widely used in diffusion codes is adopted to solve Eq. (12).

3. Results

In order to gain and enhance confidence that the 3DMOC-NSPn code has the capability in performing neutronics calculations for large-scale and complex models such as ITER TBM, some benchmarks calculations have been performed. The DFLL-TBM system, which is designed to verify and validate the relevant technologies of the helium/lithium-lead dual-cooled blanket for the Chinese fusion DEMO reactor [19], had been selected as the benchmark model.

3.1. Outline of the DFLL-TBM

The DFLL-TBM system is one of the two china breeding blanket lines selected for testing in ITER. It relies on the use of Pb–Li liquid eutectic alloy, both as tritium breeder and neutron multiplier. It should be cased with a poloidal lay-out in an ITER equatorial port and should be housed in a water-cooled steel frame directly supported by the vacuum vessel. It should be tested during the ITER high duty D-T plasma phase.

The structure of DFLL-TBM consists of a 484 mm (t) × 1660 mm (p) × 585 mm (r) rectangular steel box [13,19], which is reinforced by one radial–poloidal (r–p) and four toroidal–poloidal (t–p) stiffening plates (SPs), containing the LiPb flow channels as schematically shown in Fig. 3 [19].

First wall (FW) is designed to withstand the heat flux from the plasma chamber. According to the ITER requirements, the FW has to be covered by 2 mm thick beryllium layer, before the module can be irradiated [19]. The FW is composed of three layers FW1, FW2 and FW3 and the layout of these three layers is shown in Fig. 4. FW1

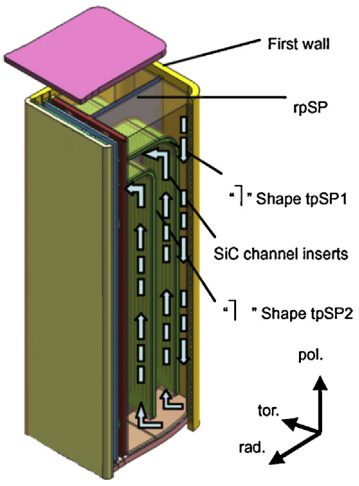

Fig. 3. 3D structure of DFLL-TBM.

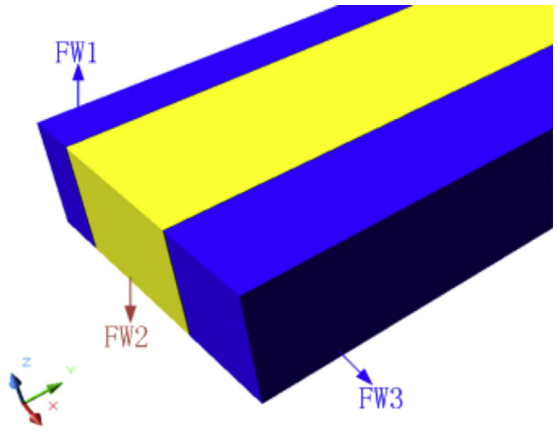

Fig. 4. Structure of FW.

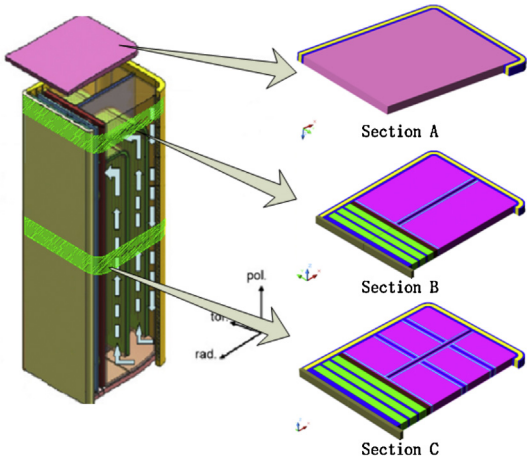

Fig. 5. Dissection processing of DFLL-TBM.

and FW3 are both made of CLAM steel. FW2 is a mixture of CLAM 20.4 vol.% and helium 79.6 vol.%.

The back plates (BPs) are designed as the strong back support for the TBM and acted as He manifold as well. The BPs are made up of two thick plates (BP1, BP4: 20 mm thick) serving as structure functions and two intermediate thin plates (BP2, BP3: 10 mm thick) serving as flow separators.

The main parameters of DFLL-TBM and the detailed materials distribution could be found in Refs. [13,19].

3.2. The modeling process and results of 3DMOC

As mentioned in Section 2, the whole DFLL-TBM was dissected into several units and the principle of this processing was based on the features of the radial structure of TBM. The whole processing procedure is shown in Fig. 5.

The Cover plate placed at the top of DFLL-TBM was modeled as shown in Section A. The layer beneath the Cover plate was dissected and modeled as Section B. The radial and poloidal structure of Section C is the representative structure of TBM and it was also modeled in AutoCAD.

These three parts in Fig. 5 were modeled in AutoCAD code separately. Subsequently, the characteristic rays' information of these parts was generated in CAD code automatically by a VBA script, adopting the modular tracing technique.

Followed by the dissection and generating of characteristic rays information were the 3D transport calculations with 3DMOC to get the ultra fine group spectra and the spatial distribution of the three typical parts in Fig. 5. Then the homogenization technique was implemented to get the homogeneous cross sections. The 175-group structure library was condensed to a smaller, more manageable energy group structure. The 14 MeV neutron source was placed on the right side besides FW1. The right side was the farthest away from the source and vacuum boundary is assumed at the side. The boundary conditions on the left sides are assumed to reflective boundaries.

Fig. 6 shows the log of the neutron flux spectra in the three First Wall zones of Section C in Fig. 5. The results obtained by 3DMOC

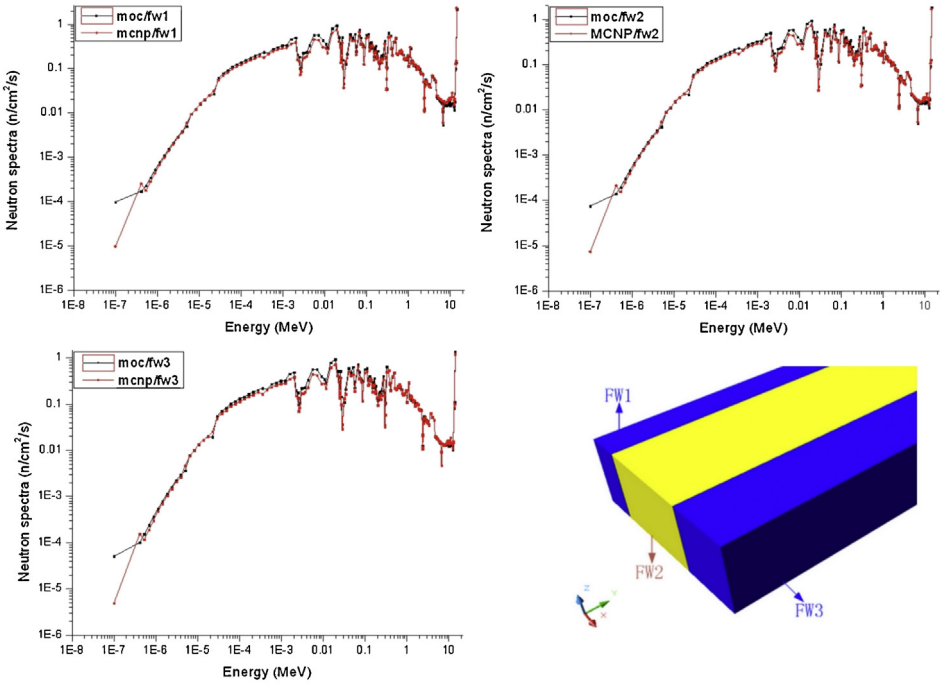

Fig. 6. Flux spectrum of FW.

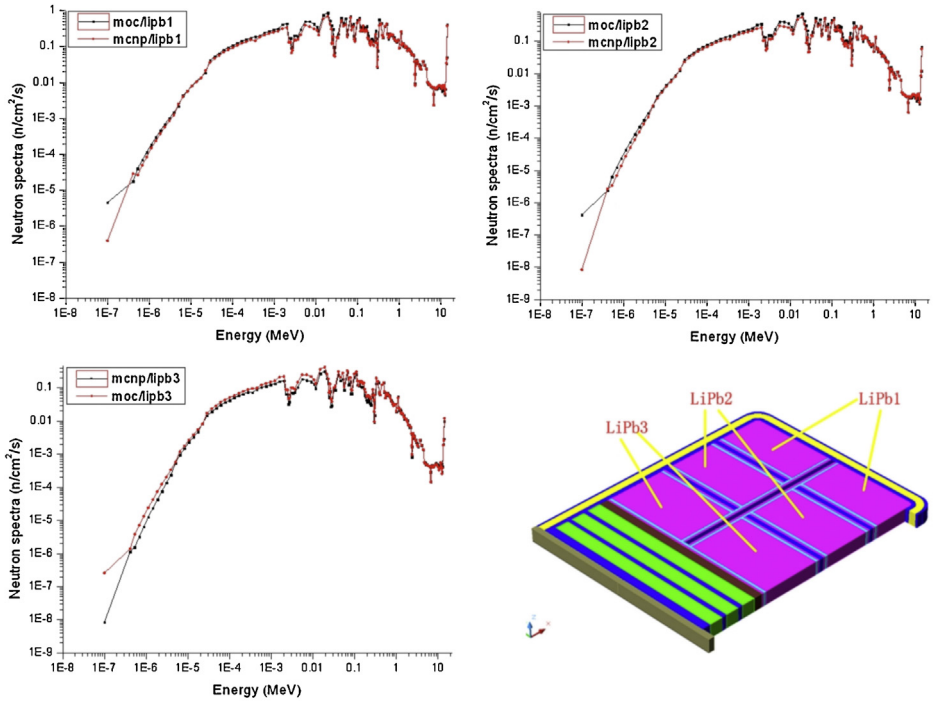

Fig. 7. Flux spectrum of three LiPb regions.

were compared with those obtained by MCNP. Fig. 7 depicts the comparison of the neutron flux in the three LiPb regions between MCNP and 3DMOC. The three LiPb zones are depicted in Fig. 7. The flux was normalized to the condition that intensity of neutron source in unit volume equals to 1.

As in Figs. 6 and 7, the neutron flux spectra obtained by 3DMOC is in good agreement with that obtained by MCNP except for the last group (the 175 group). Great percentage deviation can be observed in this group due to that the flux in this group is too small. The MCNP results here suffer large statistical errors and are not exact enough as the reference. Nonetheless, the numerical results show that the results obtained by 3DMOC are accurate enough and reliable.

3.3. The results of NSPn

In this paper, the 175 fine-group cross-section was condensed to 5 coarse-group cross-section using the method described in Section 2.3. Then the 5 group cross sections were used as input for NSPn. Fig. 8 shows the comparison of total neutron flux gained by NSPn and MCNP, respectively. The source convergence criteria used in the NSPn calculation was 10^{-3}. The results were normalized to the neutron wall load of 0.78 MW/m^2 according to the ITER Nuclear Analysis Report [20]. The agreement between NSPn and MCNP is excellent. However as shown in Fig. 8, results obtained by MCNP are higher in the region near the source, but the difference is within 10%. This region bears high energy irradiation due to the 14 MeV neutrons arising directly from the source so that the anisotropy in this region is severe. Consequently, the traditional homogenization technique will bring large biases at this region. Nevertheless, the percentage deviations are very acceptable at most regions along the radial direction.

The Tritium Breeding Rate (TBR) is an important parameter for TBM. It measures the tritium production capability of TBM. In the present paper, TBR was calculated by the following equation:

$$\mathrm{TBR} = \int_V \left[\sum_{g=1}^{5} \left(\sum_{(n,T)}^{6} + \sum_{(n,T,n')}^{7} \right) \cdot \phi_g \right] \cdot dV \qquad (14)$$

where $\sum_{(n,T)}^{6}$ and $\sum_{(n,T,n')}^{7}$ are the tritium-producing macro-cross-section of ^{6}Li and ^{7}Li, respectively. They were also condensed to 5 groups. ϕ_g is the 5 group neutron flux obtained by NSPn calculation.

The TBR obtained by MCNP and 3DMOC-NSPn were 0.338 and 0.351, respectively. The difference was 3.84%. It shows that the TBR obtained by NSPn calculation is acceptable.

During fusion plant operation, the highly energetic fusion neutrons coming out from plasma induce two main damage mechanisms [3]. The first mechanism is due to the displacement of the atoms from their lattice positions as consequence of collisions. The second mechanism is due to the gas production as result of various nuclear reactions mainly of (n, p) and (n, α) kind [3].

In order to investigate the level of DFLL-TBM material damage due to the first mechanism, the displacement per atom (DPA) was evaluated focusing the attention on the Fe^{56} isotope and adopting

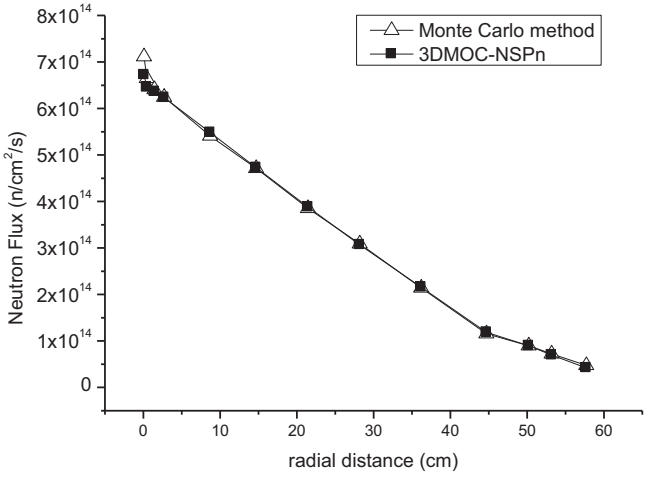

Fig. 8. Total flux along radial direction.

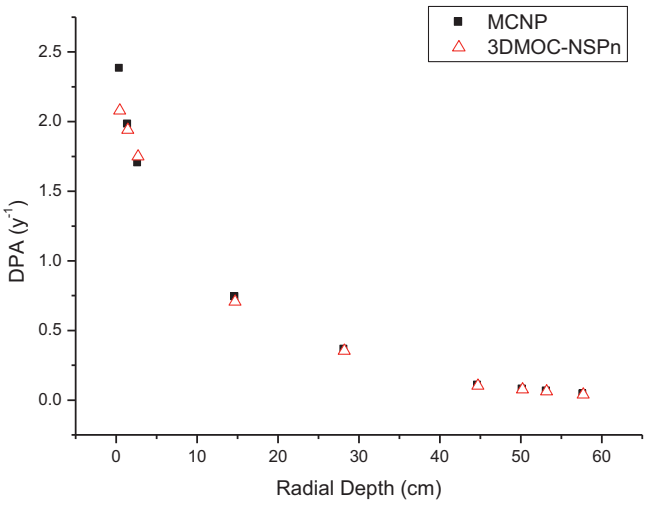

Fig. 9. Comparison of DPA radial distribution within structural material.

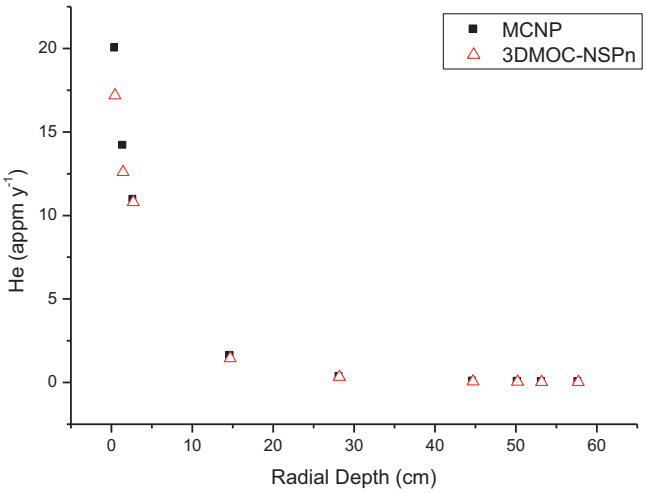

Fig. 11. Comparison of He production rate within structural material.

the displacement cross section taken from FENDL-2.1. The DPA distribution of the DFLL-TBM structural material was calculated by assuming a 0.22 duty factor (400 s burn length within a pulse of 1800 s) in a whole year. The results were normalized to the neutron wall load of 0.78 MW/m^2. Fig. 9 depicts the DPA distribution along the radial depth.

As expected, the maximum value of DPA is reached within FW1, where the neutron flux energy distribution is particularly hard due to the 14 MeV neutrons. The FW1 region also has the maximum error ~10% due to the severe anisotropy in this region. Besides FW1, the calculation errors of other regions are no more than 5%. It shows that the DPA results of 3DMOC-NSPn are acceptable.

In order to estimate the effect of the second damage mechanism, helium and hydrogen production rates were evaluated. The profiles obtained are reported in Figs. 10 and 11. As shown in Figs. 10 and 11, the maxima are reached in FW1 for helium and hydrogen, respectively. The decrease of both helium and hydrogen production rates along the radial depth is mainly due to the similar decrease of the fast neutron flux. The discrepancy values of both the two gas production rates are slightly higher in FW1 region due to the severe anisotropy as consequence of the 14 MeV neutrons. The percentage differences of the other regions are reasonable.

Both the 3DMOC calculation and the MCNP calculation were performed on a Xeon LINUX Cluster, using 2 calculation nodes. Each node has 8 processors. The NSPn calculation was accomplished on a personal computer with 4GB memories and an Intel I7 CPU. Computer time for running the 3DMOC calculation was about 18 min. In the calculation scheme, several times calculations were needed for different homogenization as shown in Fig. 5. Therefore, about 1 h was needed for the cross section condensation. After that only 6 min were needed to accomplish the NSPn calculation. Thereupon, an hour was cost to achieve the results while it took ~7 h to complete the MCNP calculation (1E8 particles; parallel computing with 16 CPUs on a LINUX parallel cluster).

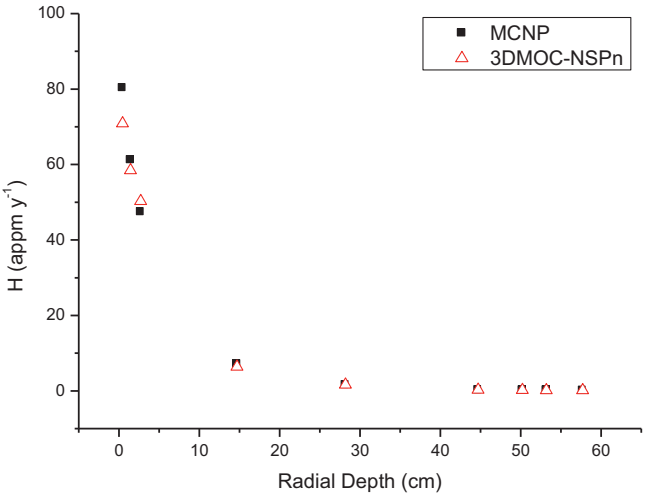

Fig. 10. Comparison of H production rate within structural material.

4. Conclusions

A new approach using the 3D deterministic methods for ITER TBM calculation have been described in this paper. In order to benchmark the new approach and the code package, the calculated results of DFLL-TBM were compared with those obtained by Monte Carlo code.

The differences between the 3DMOC-NSPn results and the Monte Carlo results are analyzed. The neutron flux spectra obtained by 3DMOC agree well with those from Monte Carlo code. As to the final total flux distribution, the differences between NSPn results and Monte Carlo results in most regions are very small except in the region that near the source. Nevertheless the largest discrepancy is no more than 10%. The reason for the discrepancy is also discussed in Section 3. The neutronics results obtained by 3DMOC-NSPn such as the TBR, the DPA, the H and the He production rate show good agreement with those obtained by Monte Carlo code. The largest biases (~10%) of these results are obtained in the region near the source. In most regions, the deviations are within 5%. It verifies that the 3DMOC-NSPn code package is feasible and correct and it keeps the computational accuracy when applied to problems with complex and heterogeneous geometries. In addition, the total computer time of the new method is much less than the one taken to accomplish the MCNP run. It confirms that this newly developed code package is significantly effective for evaluating the TBM and has great advantage in solving the time-consuming problem.

To conclude, it can be stated that the new approach shows high calculation accuracy and efficiency. It can thus be considered as a reliable new tool for the ITER-related works. However, the results also show that the traditional homogenization technique would bring biases at the regions where the anisotropy is severe. Hence, the advanced homogenization technique will be studied in future work.

Acknowledgements

This work is supported by a grant from the National Magnetic Confinement Fusion Science Program (Approved Number 2010GB111007) and financially supported by ITER project (No. 2009GB109001) and National Natural Science Foundation of China (No. 91126005).

References

[1] The IAEA Nuclear Data Section, FENDL-2.1 Fusion Evaluated Nuclear Data Library, Vienna, Austria, INDC(NDS)-467, Version December 2004.
[2] P. Chiovaro, P.A. Di Maio, G. Vella, On the nuclear response of the helium-cooled lithium lead test blanket module in ITER, Fusion Engineering and Design 75–79 (2005) 725–730.
[3] P. Chiovaro, P.A. Di Maio, G. Vella, Study of the helium-cooled lithium lead test blanket module nuclear behavior under irradiation in ITER, Fusion Engineering and Design 84 (2009) 2178–2186.
[4] G. Vella, P. Chiovaro, P.A. Di Maio, Neutronic and photonic analysis of the water-cooled Pb–17Li test blanket module for ITER-FEAT, Fusion Engineering and Design 61–62 (2002) 439–447.
[5] B. Smith, P.P.H. Wilson, M.E. Sawan, Three dimensional neutronics analysis of the ITER first wall/shield module 13, in: 22nd IEEE/NPSS Symposium on Fusion Engineering, 2007.
[6] S. Zheng, M. Chen, J. Li, Q. Zeng, L. Lu, Y. Li, et al., Neutronics analysis for the test blanket modules proposed for EAST and ITER, Nuclear Fusion 47 (2007) 1053–1056.
[7] Q. Zeng, L. Lu, A. Ding, Y. Li, H. Hu, S. Zheng, et al., Update of ITER 3D basic neutronics model with MCAM, Fusion Engineering and Design 81 (2006) 2773–2778.
[8] H. Tsige-Tamirat, U. Fischer, A. Serikov, Automatic generation and validation of an ITER neutronics model from CAD data, Fusion Engineering and Design 82 (2007) 1956–1959.
[9] J.F. Briesmeister (Ed.), MCNP4C General Monte Carlo N-Particle Transport Code, Los Alamos National Laboratory, LA-13709-M, 2000.
[10] H.P. Smith, J.C. Wagner, A case study in manual and automated Monte Carlo variance reduction with a deep penetration reactor shielding problem, Nuclear Science and Engineering 149 (2005) 23–37.
[11] X. Chai, K. Wang, The linear source approximation in three dimension characteristics method, in: International Conference on Mathematics, Computational Methods & Reactor Physics (M&C 2009), American Nuclear Society Saratoga Springs, New York, May 3–7, 2009.
[12] G.S. Lee, N.Z. Cho, 2D/1D fusion method solutions of the three-dimensional transport OECD benchmark problem C5G7 MOX, Progress in Nuclear Energy 48 (2006) 410–423.
[13] Y. Wu, The FDS Team, Design analysis of the China dual-functional lithium lead (DFLL) test blanket module in ITER, Fusion Engineering and Design 82 (2007) 1893–1903.
[14] D.L. Aldama, A. Trkov, FENDL-2.1, Update of an evaluated nuclear data library for fusion applications, Report INDC(NDS)-467, International Atomic Energy Agency, 2004.
[15] R.E. MacFarlane, TRANSX2: a code for interfacing MATXS cross-section libraries to nuclear transport codes, Technical Report LA-12312-MS, Los Alamos National Laboratory, July 1992.
[16] Z.Y. Liu, H.C. Wu, L.Z. Cao, Q.C. Chen, Y.Z. Li, A new three-dimensional method of characteristics for the neutron transport calculation, Annals of Nuclear Energy 38 (2011) 447–454.
[17] E.M. Gelbard, Simplified Spherical Harmonics equations and their use in shielding problems, WAPD-T-1182, 1961.
[18] E.W. Larsen, J.M. McMhee, J.E. Morel, The simplified PN equations as an asymptotic limit of the transport equation, Transactions of the American Nuclear Society 66 (1992) 231–247.
[19] Y. Wu, FDS Team, Conceptual design and testing strategy of a Dual Functional Lithium Lead Test Blanket Module for ITER and EAST, Nuclear Fusion 47 (2007) 1533.
[20] NAR, ITER Nuclear Analysis Report (NAR, 1998, ITER FEAT 2001 and ITER FEAT rev. 2004).